The weak covalent bond in NgAuF (Ng=Ar, Kr, Xe): A challenge for subsystem density functional theory

S. Maya Beyhan,[1,a)] Andreas W. Götz,[1,b)] Christoph R. Jacob,[2,c)] and Lucas Visscher[1,d)]
[1]*Theoretical Chemistry, Amsterdam Center for Multiscale Modeling, Vrije Universiteit Amsterdam, De Boelelaan 1083, 1081 HV Amsterdam, The Netherlands*
[2]*Laboratorium für Physikalische Chemie, ETH Zurich, Wolfgang-Pauli-Strasse 10, 8093 Zurich, Switzerland*

(Received 5 November 2009; accepted 24 December 2009; published online 28 January 2010)

We have assessed the accuracy of a representative set of currently available approximate kinetic-energy functionals used within the frozen-density embedding scheme for the NgAuF (Ng=Ar, Kr, Xe) molecules, which we partitioned into a Ng and a AuF subsystem. Although it is weak, there is a covalent interaction between these subsystems which represents a challenge for this subsystem density functional theory approach. We analyzed the effective-embedding potentials and resulting electron density distributions and provide a quantitative analysis of the latter from dipole moment differences and root-mean-square errors in the density with respect to the supermolecular Kohn–Sham density functional theory reference calculation. Our results lead to the conclusion that none of the tested approximate kinetic-energy functionals performs well enough to describe the bond between the noble gas and gold adequately. This observation contributes to the growing evidence that the current procedure to obtain approximate kinetic-energy functionals by reparametrizing functionals obtained via the "conjointness" hypothesis of Lee, Lee, and Parr [Phys. Rev. A **44**, 768 (1991)] is insufficient to treat metal-ligand interactions with covalent character. © *2010 American Institute of Physics*. [doi:10.1063/1.3297886]

I. INTRODUCTION

The increasing interest in application of quantum chemical methods in the study of biological systems has led to widespread use of subsystem methods that focus the attention on a particular region of interest, treating the environment at a lower level of theory.[1–5] Many developments were pioneered by Warshel and co-workers[6,7] who introduced the quantum mechanics/molecular mechanics (QM/MM) method and later introduced an approach in which a local pseudopotential representing the environment is used to embed an active solvent molecule. In the latter scheme the pseudopotential needs to be parametrized for the solvent-solute interaction, a requirement that is not necessary in a related subsystem approach, the so-called frozen-density embedding (FDE) method within density functional theory (DFT), as proposed by Wesolowski and Warshel[8] in 1993. In this method the electron density of the environment is included in the calculation by means of an effective embedding potential that describes the difference between the full and the active system. This method can be used to calculate molecular properties of solvated systems[9–11] and, in its generalization to time-dependent DFT,[12,13] to describe local electronic excitations and couplings between such excitations.[14–17] The method can also be used to compute interaction energies of weakly interacting systems[18–21] as well as strong interaction energies as in ligand-metal bonds[21] or to optimize structures of such complexes,[22] and has also been explored in molecular dynamics simulations.[23,24] The FDE method as well as other relevant methods to describe biological systems are recently reviewed by Kamerlin *et al.*[25]

The foundation of FDE is a subsystem formulation of DFT.[26] In most cases the density is partitioned into two subdensities that each corresponds to an integer number of electrons, but a three-partitioning scheme that uses capping atoms to enable fractionation of strongly interacting subsystems has also been developed.[27] In FDE, the density $\rho^{(1)}(\boldsymbol{r})$ of an active fragment is determined in the presence of an effective embedding potential due to the frozen electron density $\rho^{(2)}(\boldsymbol{r})$ of the environment. Provided that an initial guess for the environment density $\rho^{(2)}(\boldsymbol{r})$ is available, Kohn–Sham (KS)-like one-electron equations can be obtained for the determination of this active density $\rho^{(1)}(\boldsymbol{r})$ from the minimization of the energy functional $E=E[\rho^{(1)},\rho^{(2)}]$ with respect to $\rho^{(1)}(\boldsymbol{r})$, while keeping $\rho^{(2)}(\boldsymbol{r})$ frozen.[8,28] To stress the difference with regular KS approaches these one-electron equations can be called the KS equations with constrained electron density (KSCED). For doubly occupied orbitals $\phi_i^{(1)}(\boldsymbol{r})$ of subsystem (1) they read

$$\left[-\frac{\nabla^2}{2}+v_{\mathrm{eff}}^{\mathrm{KSCED}}[\rho^{(1)},\rho^{(2)}](\boldsymbol{r})\right]\phi_i^{(1)}(\boldsymbol{r})=\epsilon_i\phi_i^{(1)}(\boldsymbol{r}),\quad i=1,\ldots,\frac{N^{(1)}}{2}. \tag{1}$$

The effective potential in these equations is given by

[a)]Electronic mail: mbeyhan@few.vu.nl.
[b)]Electronic mail: agoetz@sdsc.edu. Present address: San Diego Supercomputer Center, University of California San Diego, 9500 Gilman Drive MC0505, La Jolla, CA 92093-0505, USA.
[c)]Electronic mail: christoph.jacob@phys.chem.ethz.ch.
[d)]Electronic mail: visscher@chem.vu.nl.

$$v_{\mathrm{eff}}^{\mathrm{KSCED}}[\rho^{(1)},\rho^{(2)}](\boldsymbol{r}) = v_{\mathrm{eff}}^{\mathrm{KS}}[\rho^{(1)}](\boldsymbol{r}) + v_{\mathrm{eff}}^{\mathrm{emb}}[\rho^{(1)},\rho^{(2)}](\boldsymbol{r}), \tag{2}$$

where $v_{\mathrm{eff}}^{\mathrm{KS}}[\rho^{(1)}](\boldsymbol{r})$ is the KS effective potential of the isolated subsystem 1 containing the usual terms of the nuclear potential, the Coulomb potential of the electrons, and the exchange-correlation (XC) potential,

$$v_{\mathrm{eff}}^{\mathrm{KS}}[\rho^{(1)}](\boldsymbol{r}) = v_{\mathrm{nuc}}^{(1)}(\boldsymbol{r}) + \int \frac{\rho^{(1)}(\boldsymbol{r}')}{|\boldsymbol{r}-\boldsymbol{r}'|}d\boldsymbol{r}' + \left.\frac{\delta E_{\mathrm{XC}}[\rho]}{\delta\rho}\right|_{\rho=\rho^{(1)}(\boldsymbol{r})}. \tag{3}$$

The effect of subsystem 2 is represented by the effective-embedding potential $v_{\mathrm{eff}}^{\mathrm{emb}}[\rho^{(1)},\rho^{(2)}](\boldsymbol{r})$ that reads

$$v_{\mathrm{eff}}^{\mathrm{emb}}[\rho^{(1)},\rho^{(2)}](\boldsymbol{r}) = v_{\mathrm{nuc}}^{(2)}(\boldsymbol{r}) + \int \frac{\rho^{(2)}(\boldsymbol{r}')}{|\boldsymbol{r}-\boldsymbol{r}'|}d\boldsymbol{r}' + \left.\frac{\delta E_{\mathrm{XC}}[\rho]}{\delta\rho}\right|_{\rho=\rho^{(\mathrm{tot})}(\boldsymbol{r})} - \left.\frac{\delta E_{\mathrm{XC}}[\rho]}{\delta\rho}\right|_{\rho=\rho^{(1)}(\boldsymbol{r})} + \left.\frac{\delta T_{\mathrm{s}}[\rho]}{\delta\rho}\right|_{\rho=\rho^{(\mathrm{tot})}(\boldsymbol{r})} - \left.\frac{\delta T_{\mathrm{s}}[\rho]}{\delta\rho}\right|_{\rho=\rho^{(1)}(\boldsymbol{r})}, \tag{4}$$

where $v_{\mathrm{nuc}}^{(2)}(\boldsymbol{r})$ denotes the external potential due to the nuclei of system 2, $\rho^{(\mathrm{tot})}(\boldsymbol{r})=\rho^{(1)}(\boldsymbol{r})+\rho^{(2)}(\boldsymbol{r})$ is the electron density of the whole system, $T_{\mathrm{s}}[\rho]$ is the functional for the kinetic energy (KE) of the noninteracting reference system defined in the KS theory, and $E_{\mathrm{XC}}[\rho]$ is the functional for the XC energy.

The formalism assumes that for a given $\rho^{(2)}(\boldsymbol{r})$, the active density $\rho^{(1)}(\boldsymbol{r})=\rho^{(\mathrm{tot})}(\boldsymbol{r})-\rho^{(2)}(\boldsymbol{r})$ is non-negative everywhere in space and noninteracting v_{s}-representable.[28,29] In that case the supermolecular KS-DFT results for a given approximate functional for $E_{\mathrm{XC}}[\rho]$ should be reproduced by the subsystem calculation, provided that the exact KE functional $T_{\mathrm{s}}[\rho]$ is used. In practice the first condition is difficult to fulfill exactly with a simple trial density, making it necessary to introduce the so-called "freeze-and-thaw" (FT) procedure[30] in which both densities are adjusted in an iterative fashion. More importantly, the exact $T_{\mathrm{s}}[\rho]$ is unknown and one has to resort to an approximant for the nonadditive KE and the KE component of the embedding potential. Wesolowski and co-workers[19,20,31–34] examined such approximate KE functionals in the FDE scheme and showed that with generalized-gradient approximation (GGA) functionals, accurate results are obtained for a variety of weakly interacting systems.[19,33,34] A similar conclusion was reached by Kiewisch *et al.*[29] who studied also the strongly hydrogen-bonded system F–H–F$^-$.[29] Recently, however, Fux *et al.*[35] analyzed the electron density distributions from FDE calculations on subsystems connected by coordination bonds. They show that FDE, with a GGA approximation to the KE component of the embedding potential, fails for compounds with strong covalent bonding contributions.

In an earlier study,[36] an exact form for the nonadditive KE component of the effective embedding potential $v_{\mathrm{eff}}^{\mathrm{emb}}[\rho^{(1)},\rho^{(2)}](\boldsymbol{r})$ at the long-distance limit has been derived and a position-dependent correction has been proposed which ensures the correct behavior for this KE component in this limit. This correction has been shown to lead to an improved description of covalent bonds in transition metal complexes, even though the resulting density is still not very accurate.[35] More recently, an approximation for the nonadditive KE component has been constructed which enforces the exact limit near nuclei in the environment.[37]

Our goal is to analyze the behavior of the currently available GGAs that underlie both the older and the newer generations of the nonadditive KE functionals. These functionals are constructed following successful exchange functional forms, in line with the conjointness hypothesis of Lee, Lee, and Parr (LLP).[38] In our analysis, we also include the PBE*n* KE functionals developed by Karasiev *et al.*[39] that have only recently been tested in the context of FDE.[21]

The present study was designed to assess the NgAuF (Ng=Ar, Kr, Xe) molecules in which the bond between the noble gas and AuF has a considerably covalent character[40,41] and for which we may tune the interaction strength by changing the coordinating noble gas atom. Another advantage of this type of molecules is their linearity, making it easy to visualize the embedding potentials and deformation densities along the bond axis.

In Sec. II, we briefly discuss the available approximate KE functionals and the conjointness conjecture. Section III contains details on the computational methods applied in this work. Section IV is devoted to discussion of the results. In Sec. IV A, we examine the differences between the embedding potentials calculated using different approximations for the nonadditive KE functional. In Sec. IV B, we consider the induced dipole moments of the Ng (Ng=Ar, Kr, Xe) atoms that are obtained without relaxing the density of the AuF unit. In Sec. IV C, we allow for this relaxation using the FT procedure, and in Sec. IV D we quantify the differences of the obtained total density with respect to the supermolecular reference density. Finally, concluding remarks are given in Sec. V.

II. APPROXIMATE KINETIC-ENERGY FUNCTIONALS

The simplest approach to describe the KE in terms of a density functional is the Thomas–Fermi (TF) model.[42–44] The TF model has well-known defects in the description of the total KE of molecules[45–48] but yields a reasonable approximation to the repulsive part of the embedding potential to be of use as a starting point for the FDE approach. The TF KE functional is given by

$$T_{\mathrm{TF}}[\rho] = C_{\mathrm{TF}}\int \rho^{5/3}(\boldsymbol{r})d\boldsymbol{r}, \quad C_{\mathrm{TF}} = \frac{3}{10}(3\pi^2)^{2/3} \approx 2.871, \tag{5}$$

where C_{TF} is the TF constant. This local density approximation of the KE is exact for the uniform-electron gas.

Another simple model was developed by von Weizsäcker (vW) (Ref. 49) based on another exact limit: the KE density functional for two-electron systems. This functional is defined by the equation

$$T_{\mathrm{vW}}[\rho] = \frac{1}{8}\int \frac{|\nabla\rho(\boldsymbol{r})|^2}{\rho(\boldsymbol{r})}d\boldsymbol{r}. \tag{6}$$

The vW functional should be applicable in the outer regions of a molecule and close to the nuclei, where the density can be considered to be due to a single orbital. Since it gives zero KE in the uniform-electron gas limit it can be included as a correction to the TF KE. This gives the Thomas–Fermi–von Weizsäcker model (TFW),

$$T_{\mathrm{TFW}}[\rho] = T_{\mathrm{TF}}[\rho] + \lambda T_{\mathrm{W}}[\rho], \tag{7}$$

where λ is a parameter with $0 \leq \lambda \leq 1$. The standard value $\lambda = 1/9$ follows from a second-order gradient expansion of the KE. The TFW model has been shown to be able to improve the overall accuracy relative to the individual functionals, but the errors in the total KE are still too large to be used in quantitative calculations.

Further sophistications can be introduced to model deviations from the uniform-electron gas limit by including the gradients of the density in GGA functionals. Modern developments thereby usually follow the idea of LLP who conjectured the concept of "conjointness"[38] of the scale invariant part of the kinetic and exchange energy expressions. This idea has been widely adopted with examples given in Refs. 50–54. According to the LLP conjointness concept, KE functionals are written in the form of a GGA,[55]

$$T_{\mathrm{s}}^{\mathrm{GGA}}[\rho] = C_{\mathrm{TF}}\int \rho^{5/3}(\boldsymbol{r})F_{\mathrm{t}}(s(\boldsymbol{r}))d\boldsymbol{r}, \tag{8}$$

where the dimensionless function $F_{\mathrm{t}}(s)$ is called the "enhancement factor" and the reduced density gradient is denoted by $s \equiv |\nabla\rho|/(2\rho k_{\mathrm{F}})$ with $k_{\mathrm{F}} = (3\pi^2\rho)^{1/3}$. For the enhancement factor one then uses the same functional form as for approximate exchange functionals, i.e.,

$$F_{\mathrm{t}}(s(\boldsymbol{r})) \approx F_{\mathrm{x}}(s(\boldsymbol{r})). \tag{9}$$

In practical orbital-free DFT (and FDE) calculations the parameters in the enhancement factor are often refitted to yield an improved description of the (nonadditive) KE and its functional derivative, the kinetic contribution to the (embedding) potential. In this work we will compare the behavior of five different GGA functionals based on this conjointness concept.

The PW91K GGA KE functional[20,50] has the same functional form for the enhancement factor $F(s)$ as the exchange functional of Perdew and Wang (PW91),[56] and was parametrized for the KE by Lembarki and Chermette[50] as

$$F_{\mathrm{t}}^{\mathrm{PW91K}}(s) = \frac{1 + A_1 s\,\sinh^{-1}(As) + (A_2 - A_3 e^{-A_4 s^2})s^2}{1 + A_1 s\,\sinh^{-1}(As) + B_1 s^4}, \tag{10}$$

with $A_1 = 0.093\,907$, $A_2 = 0.266\,08$, $A_3 = 0.080\,961\,5$, $A_4 = 100.00$, $A = 76.320$, and $B_1 = 0.577\,67 \times 10^{-4}$.

This functional form of the KE is useful for embedding purposes because $F_{\mathrm{t}}^{\mathrm{PW91K}}(s)$ smoothly approaches zero as s becomes large.[28] This makes the KE contribution to the embedding potential positive in regions of low density of the active subsystem since the last term of Eq. (4) remains small.

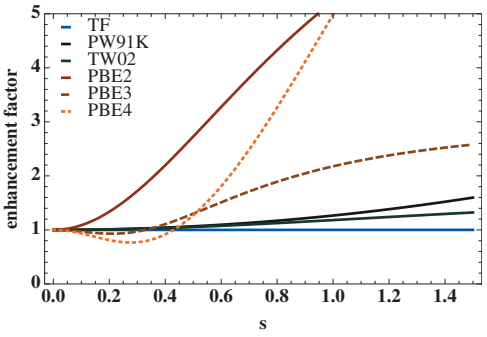

FIG. 1. Enhancement factors used in KE functionals plotted in the domain $0.0 < s < 1.5$. To guide the eye we also display the constant value of 1 that corresponds to the original TF ansatz.

The PW91 enhancement factor is, however, rather complicated. For XC functionals it is often replaced by the simple function introduced for E_{x} by Becke and used by Perdew, Burke, and Ernzerhof (PBE) in their XC functional.[57] This enhancement function,

$$F_{\mathrm{t}}^{\mathrm{PBE}}(s) = 1 + \frac{C_1 s^2}{1 + a_1 s^2}, \tag{11}$$

has also been reparametrized for use in KE functionals. Tran and Wesolowski[54] fitted the parameters to reproduce the exact KE of the He and Xe atoms and developed the Tran–Wesolowski (TW02) functional that has $C_1 = 0.2319$ and $a_1 = 0.2748$. Karasiev *et al.*[39] chose to reproduce the KS forces of a training set of silicon oxide molecules, irrespective of the resulting total energy. Since the total KE is not of interest in FDE calculations (as the bulk of the energy is given by the KS expression), and because the functional derivative appearing in the force expression also appears in the expression for the embedding potential, this ansatz may also be interesting in the present context. The resulting parameters ($C_1 = 8.7575$ and $a_1 = 1.0706$) are substantially larger than the TW02 parametrization making this PBE2 functional deviate considerably from the TF starting point. It is thus interesting to see what such a larger departure from the TF starting point may give, although we should keep in mind that the training set (silicon oxide bonds) used by Karasiev and co-workers is quite different from the weak covalent bonding that we are aiming to treat.

The same authors[39] also developed three- and four-parameter enhancement factors $F(s)$ (dubbed PBE3 and PBE4, respectively, by them) based on the expressions introduced by Adamo and Barone,[58]

$$F_{\mathrm{t}}^{\mathrm{PBEn}}(s) = 1 + \sum_{i=1}^{n-1} C_i^{(n)}\left[\frac{s^2}{1 + a_1^{(n)} s^2}\right]^i, \tag{12}$$

with $C_1^{(3)} = -3.7425$, $a_1^{(3)} = 4.1355$ and $C_2^{(3)} = 50.258$, and $C_1^{(4)} = -7.2333$, $a_1^{(4)} = 1.7107$, $C_2^{(4)} = 61.645$, and $C_3^{(4)} = -93.683$.

In contrast to the functions discussed earlier, the PBE3 and PBE4 enhancement factors may attain values smaller than 1 for small values of s, thus reducing the TF KE density rather than enhancing it. This difference between the enhancement factors is displayed in Fig. 1. Apart from the

small *s* behavior of PBE3 and PBE4 one may also note the similarity between the PW91K and TW02 enhancement functions.

III. COMPUTATIONAL DETAILS

All calculations were performed using the FDE (Ref. 8) implementation[15,59] in the Amsterdam density functional (ADF) package.[60,61] The PBE XC functional,[57] the zeroth order regular approximation,[62,63] and the TZ2P basis set from the ADF basis set library[61] were employed throughout this work. FDE calculations were performed using both the default basis set expansion [denoted as FDE(m)], in which only the basis functions of the active subsystem are used, and the supermolecular basis set expansion [denoted as FDE(s)],[20] in which the basis functions of both subsystems are used. If not stated otherwise, electron densities of both subsystems were relaxed and converged in six FT cycles.[30] The approximate KE functionals for the nonadditive KE used in this work are the TF functional,[42–44] the TF plus 1/9 von Weizsäcker (TF9W) functional,[49] the PW91K functional,[20,50] the TW02 functional,[54] and the Karasiev–Trickey–Harris PBE2, PBE3, PBE4 functionals.[39] These PBE*n* KE functionals were implemented in ADF for this work. For the purpose of analysis we also employed a purely electrostatic embedding (EE) in which the embedding potential contained only the Coulomb interaction with the frozen system, that is, omitting the nonadditive KE and XC energy contributions.

The electron density and the quantities derived from it were obtained on the integration grid used by ADF from a locally modified version of the DENSF-utility program of the ADF package. For visualization, the electron deformation density, the enhancement factor, and the effective embedding potential were obtained on an evenly spaced grid by the same locally modified version of DENSF. The electron deformation density $\rho_{\mathrm{def}}(\boldsymbol{r})$ is defined as

$$\rho_{\mathrm{def}}(\boldsymbol{r}) = \rho_{\mathrm{SCF}}(\boldsymbol{r}) - \rho^{(1)}_{\mathrm{frag}}(\boldsymbol{r}) - \rho^{(2)}_{\mathrm{frag}}(\boldsymbol{r}), \tag{13}$$

where $\rho^{(i)}_{\mathrm{frag}}(\boldsymbol{r})$ $(i=1,2)$ is the electron density of an isolated fragment and $\rho_{\mathrm{SCF}}(\boldsymbol{r})$ the final converged self-consistent field (SCF) electron density. In the case of FDE, we have $\rho_{\mathrm{SCF}}(\boldsymbol{r})=\rho^{(\mathrm{tot})}_{\mathrm{FDE(6)}}(\boldsymbol{r})=\rho^{(1)}_{\mathrm{FDE(6)}}(\boldsymbol{r})+\rho^{(2)}_{\mathrm{FDE(6)}}(\boldsymbol{r})$. In order to quantitatively visualize the deformation density along the bond axis (*z*-axis), we adopted a scheme inspired by the one employed by Belpassi *et al.*[41] We numerically integrated on the evenly spaced grid used by DENSF (integration accuracy of 10^{-4} a.u. for the electron deformation density) over the *x*- and *y*-coordinates for every corresponding point on the *z*-axis,

$$\tilde{\rho}(z) = \int_{-\infty}^{\infty}\int_{-\infty}^{\infty} \rho_{\mathrm{def}}(x,y,z)dxdy. \tag{14}$$

This condenses the information contained in these three-dimensional functions to one-dimensional functions that are easier to plot. Since results of the calculations with the supermolecular basis set expansion were very similar, all the figures throughout this work display the data obtained with the default monomolecular basis set expansion.

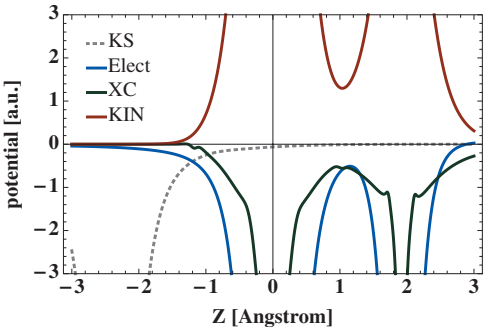

FIG. 2. ArAuF: the KS potential and contributions of the embedding potential due to electrostatic (nuclear and Coulomb), nonadditive XC and KE for the TF KE functional along the bond axis. The Au atom is situated at $z=0.0$ Å, F at $z=1.92$ Å, and Ar at $z=-2.39$ Å.

For each Ng–AuF (Ng=Ar, Kr, Xe) molecule, the calculations were done at a single geometry, with bond lengths taken from the analysis of experimental microwave data. The Ng–Au distances are $d(\mathrm{Ar-Au})=2.391$,[64] $d(\mathrm{Kr-Au})=2.461$,[65] and $d(\mathrm{Xe-Au})=2.543$ Å,[40] while the AuF distance was fixed at 1.918 Å.[41]

IV. RESULTS AND DISCUSSION

The Ng–Au bonds in NgAuF complexes are weakly covalent, with the interaction strength increasing from 49 to 94 kJ/mol upon moving from Ar to Xe.[41] In Sec. IV A we consider only the ArAuF molecule, but quantitative differences among NgAuF molecules are discussed in Secs. IV B and IV D. Since the Ng–Au bond is much weaker than the Au–F bond (computed as 296 kJ/mol for the free molecule[41]), this naturally calls for a partitioning into Ng and AuF fragments in FDE with the Ng atom taken as the active subsystem and AuF taken as the frozen subsystem. When we consider the Ng–Au bond formation in this framework, electron density should move from the Ng atom into the bonding region (for details, see Ref. 41). This process can in principle be described by the FDE approach, possibly with the aid of the FT update procedure to allow for some adjustment of the AuF density.

A. Embedding potentials

For fixed densities and XC functional, any difference in the embedding potential $v^{\mathrm{emb}}_{\mathrm{eff}}[\rho^{(1)},\rho^{(2)}](\boldsymbol{r})$ is due only to differences in the approximate KE functional that is used. We begin our analysis by taking the density of the isolated fragments to calculate the embedding potential $v^{\mathrm{emb}}_{\mathrm{eff}}$ as well as its components [see Eq. (4)]. This corresponds to the embedding potential as it is used in the first iteration of a self-consistent solution of the KSCED equation (1).

Figure 2 shows a plot of the components of $v^{\mathrm{emb}}_{\mathrm{eff}}(\boldsymbol{r})$ for the Ar atom along the bond axis for the TF KE density functional. Figures 3 and 4 show the plots of the full embedding potential for the KE functionals investigated in this work.

At large distances from the frozen AuF unit (for $z<-2.0$ Å) all embedding potentials are dominated by the attractive electrostatic contribution. The employed (semi)local nonadditive KE and the nonadditive XC potentials approach zero because the derivatives in Eq. (4) are

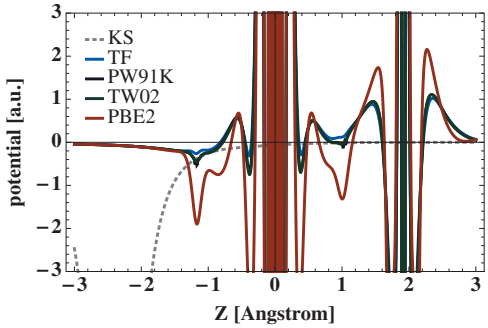

FIG. 3. ArAuF: the KS and embedding potentials generated using the TF, PW91K, TW02, and PBE2 functionals along the bond axis. The Au atom is situated at $z=0.0$ Å, F at $z=1.92$ Å, and Ar at $z=-2.39$ Å.

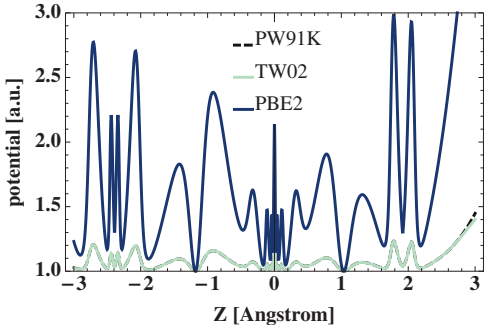

FIG. 5. ArAuF: enhancement factor for the total (sum of fragments) density, i.e., $\rho^{\mathrm{Ar}}+\rho^{\mathrm{AuF}}$, for different approximations along the bond axis. The Au atom is situated at $z=0.0$ Å, F at $z=1.92$ Å, and Ar at $z=-2.39$ Å.

evaluated at the same value of ρ when $\rho^{(2)}(\boldsymbol{r})$ is negligibly small. The other extreme is found in the vicinity of the frozen nuclei where we find an oscillatory potential resulting from competition between the large positive KE contribution and the strongly negative Coulomb potential. This highly oscillatory potential resulting from relatively smooth individual components (cf. Fig. 2 for the components and the blue line in Fig. 3 for the resulting TF embedding potential) is consistent with the assumption made in the FDE ansatz in which the active density should complement the frozen density to yield the exact total density. In the case of a heavy atom with a pronounced shell structure, such oscillatory potentials should represent the Pauli repulsion that arises due to the frozen core orbitals. This core region is overall repulsive with the shallow negative regions outweighed by regions in which the total potential is strongly positive.

The region of interest is the area between $z=-2.0$ Å and $z=-0.5$ Å in which the charge transfer from the noble gas to the AuF is known to take place and where subtle differences between the KE contributions yield an important contribution to the relatively shallow potential. To put this contribution in perspective we have also included the KS potential of the isolated Ar atom to which this embedding potential will be added in the plots. The TF curve climbs almost monotonically with the repulsive wall starting at about -1.0 Å. The PW91K and TW02 functionals deepen the well somewhat and introduce some substructure. This is amplified by the PBE*n* functionals of which we showed only the PBE2 functional together with the other GGA functionals to not clutter Fig. 3. This functional gives rise to a significant deepening of the well near the gold atom and also renders the potential in the region between the gold and the fluoride attractive. The use of higher-order terms in PBE3 and PBE4 is depicted in Fig. 4 in which we observe oscillations also in the bonding region of the complex.

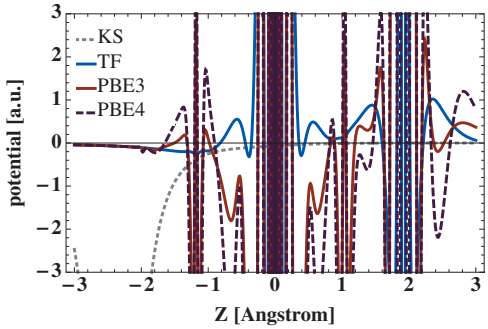

FIG. 4. ArAuF: the KS potential and embedding potentials generated using the TF, PBE3, and PBE4 functionals along the bond axis. The Au atom is situated at $z=0.0$ Å, F at $z=1.92$ Å, and Ar at $z=-2.39$ Å.

To show the cause of these differences in embedding potentials more clearly, Fig. 5 shows the enhancement factor $F_{\mathrm{t}}(s)$ for the total (sum of fragments) density of the complex, i.e., $\rho^{\mathrm{Ar}}(\boldsymbol{r})+\rho^{\mathrm{AuF}}(\boldsymbol{r})$, for different approximations of the nonadditive KE functionals.

It is the derivative of the enhancement factor with respect to the density which determines the potential. The trends observed in the embedding potential are indeed visible in the enhancement factor plots, with the PW91K and TW02 curves varying smoothly compared with the PBE2 functional that differs only in parametrization but not in functional form from TW02. Interesting is the great similarity between the PW91K and TW02 curve that deviate only in the uninteresting high s regime that starts at the low density tail of the fluoride and argon (not visible in this plot). We do not show the enhancement factor of PBE3 and PBE4 because these exhibit strong oscillations and would clutter the figure. Already from the potential, it is clear, however, that we may expect a stronger charge transfer for the PBE*n* functionals than for the other functionals.

B. Induced dipole moments

As a simple direct measure of the changes in the electron density, we take the dipole moment changes that occur upon the formation of the Ng–AuF (Ng=Ar, Kr, Xe) molecules. This property is ideally suited to assess the accuracy of the electron density that results from FDE calculations, both in comparison to the reference KS method as well as in relation to simple electrostatic models. For the latter we consider a simple model that neglects charge transfer and takes the electric field strength at the position of the Ng atom to compute an induced dipole moment $\mu^{\mathrm{ind}}=\mathbf{E}\alpha$ using the relation between this electric field strength $\mathbf{E}$ and the dipole polarizability α of the atom. The experimental values for the polarizability of the noble gas atoms were used, as obtained from Ref. 66, while the electric field was obtained by numerically differentiating the electrostatic potential due to the AuF subsystem at the position of the nucleus of the noble gas atom.

TABLE I. Magnitude of the induced dipole moments in debye of Ar, Kr, and Xe due to the interaction with the AuF molecule with different approximations. The KS induced dipole moment is obtained by subtracting the permanent dipole moment of AuF from the dipole moment of the Ng–AuF complex.

	Ar	Kr	Xe	Ar	Kr	Xe
KS				1.80	2.15	2.67
PP	0.10	0.14	0.20			
		FDE(m)			FDE(s)	
EE[a]	1.43	5.81	8.41	···	···	···
TF	0.27	0.36	0.33	0.26	0.30	0.31
TF9W	0.37	0.54	0.61	0.39	0.49	0.58
PW91K	0.36	0.52	0.57	0.39	0.49	0.56
TW02	0.36	0.53	0.58	0.41	0.50	0.58
PBE2	1.09	1.99	2.61	1.78	2.26	2.88
PBE3[a]	1.15	2.29	3.13	···	···	···
PBE4[a]	1.72	3.99	5.46	···	···	···

[a]FDE(s): SCF convergence could not be reached.

This simple point polarizability model will be denoted (PP) and can also be compared with the EE model in which the nonadditive KE and XC contributions are completely neglected in the KSCED iterations. Table I compares the induced dipole moments of Ng (Ng=Ar, Kr, Xe) molecules calculated using these models with the ones calculated with the reference KS and approximate FDE schemes.

As expected, the induced dipole moment increases from Ar to Xe due to the larger polarizability that overcomes the greater bond distance. For a system which exhibits a considerable covalent character like Xe–AuF, the PP model clearly predicts a too small effect. Missing in the PP model is the charge transfer from the Ng atom to the AuF unit, as explained in detail by Belpassi *et al.*[41] Since FDE allows for such charge transfer, we may check how much FDE does improve upon the classical model. This cannot lead to a perfect agreement as there is a small region close to the gold nucleus in which the AuF frozen density exceeds that of the NgAuF complex (the integrated negative densities are -0.051, -0.064, and -0.084 for Ng=Ar, Kr, and Xe, respectively). Adjustment of the AuF density by FT cycles to allow for this effect will be considered in Sec. IV C, but for the present qualitative purpose it is reasonable to assume that these small regions of negative density do not influence the result too much. This is also consistent with the experimental evidence that the Ng–Au bonding hardly influences the strong AuF bond much.[40,64,65] As can be seen from Table I, the TF, TF9W, PW91K, and TW02 functionals underestimate the dipole moment change for all noble gases in the series, Ar, Kr, and Xe, but do improve upon the PP model. The underestimation is not due to basis set deficiencies as calculation with the FDE(s) approach (in which the supermolecular basis is used) yields values close to the FDE(m) values. This indicates that the embedding potential generated with these functionals is too shallow, overestimating the Pauli repulsion that arises from the AuF unit.

The deeper well generated by PBE2 and PBE3 leads to dipole moment changes that approach the results of supermolecular KS calculations. The PBE2 functional gives values close to the reference result if the FDE(s) expansion, in which the basis set is equal to the one used in the reference KS calculation, is used. On the other hand one may observe that the more complicated embedding potential generated with the PBE4 functional is too attractive, leading to dipole moment changes that are well above those obtained by the KS method. Removing the repulsive nonadditive KE and XC terms by considering only EE results in a large overestimation of the charge transfer. These values provide an indication of the upper limit of charge transfer that is possible within the monomolecular expansion used in the FDE(m) approach. For the EE model, as well as for the PBE3 and PBE4 functionals, it was not possible to reach convergence in the FDE(s) expansion that allows full charge transfer to the AuF unit.

C. Deformation densities

We now allow for adjustment of the AuF density as well and define deformation densities as explained in Sec. III. After six FT cycles, the electron densities hardly change, and the quantities discussed here are converged within the reported accuracy. In order to assess the performance of these FDE deformation densities we compared them with the KS deformation density defined as $\rho^{\mathrm{KS}}(\boldsymbol{r})-\rho^{(1)}_{\mathrm{frag}}(\boldsymbol{r})-\rho^{(2)}_{\mathrm{frag}}(\boldsymbol{r})$, where $\rho^{\mathrm{KS}}(\boldsymbol{r})$ designates the density of the supermolecule obtained with the conventional KS method. These deformation densities for Ar–AuF, radially integrated and plotted along the bond axis (see Sec. II for details), are presented in Fig. 6. Because of its complicated structure, the deformation density obtained for the PBE4 functional is omitted. It deviates significantly from the KS deformation density.

In the KS deformation density, there is a sharp increase at the very center of the noble gas delimited on both sides by a decrease. The increase in density at the noble gas nucleus is due to the empty 4s orbital of Ar that participates in the molecular orbitals of the complex, resulting in a larger s-orbital occupation on the noble gas. The decrease on both sides is caused by donation from the occupied 3p orbital that participates in the weak sigma bond to the gold center. Together, this corresponds to an overall charge transfer from Ar to AuF and decrease in the density near the Ar nucleus. The

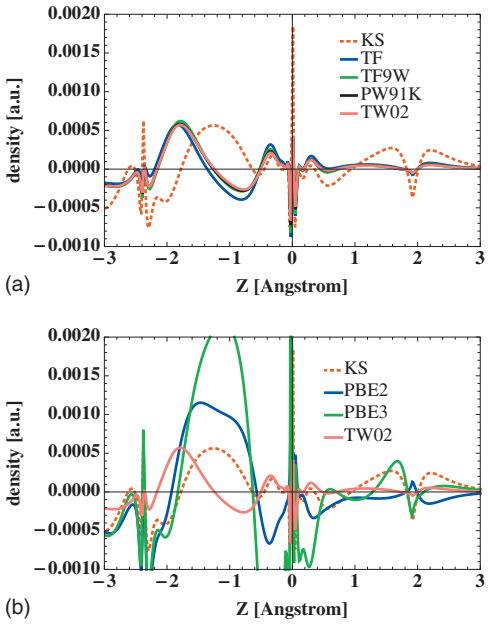

FIG. 6. Radially integrated deformation densities for different approximations of the nonadditive KE functional for the ArAuF molecule. KS denotes the difference between the KS supermolecular density and the one of sum of fragments. FDE deformation densities are calculated by taking the difference between the KSCED and sum of fragments density. The Au atom is situated at $z=0.0$ Å, F at $z=1.92$ Å, and Ar at $z=-2.39$ Å.

TF, TF9W, PW91K, and TW02 functionals all capture this trend but underestimate its magnitude with a maximum of charge buildup in the bonding region at $z=-1.8$ Å, rather than at $z=-1.1$ Å as in the KS reference. The PBE2, PBE3, and PBE4 functionals overestimate the magnitude of charge transfer. Among all functionals, PBE2 comes closest to the KS results if we look only at the density changes near Ar and in the bonding region. The picture changes when considering also the density changes near the Au center. TF, TF9W, PW91K, and TW02 now resemble the KS picture, although again underestimating the magnitude of the density distortion. The PBE2, PBE3, and PBE4 (not shown in the picture) functionals show a too complicated density deformation. Finally, in the vicinity of the fluorine nucleus, all the functionals tested here, except for PBE2, capture qualitatively the trends. Again the first family of functionals (TF, TF9W, PW91K, and TW02) underestimates the density changes, while the PBE3 functional has a very good agreement with the KS result and the PBE4 functional (not shown in the picture) overestimates it.

D. Quantitative analysis

To quantify the performance of the approximate nonadditive KE functionals under consideration, we used three measures of accuracy (see Refs. 27 and 67), again using the supermolecular KS method as a reference and considering the density after six FT cycles. The measures are the dipole moment differences for the total system,

$$\Delta\mu = \int (\rho^{\mathrm{KS}}(\boldsymbol{r}) - (\rho^{(1)}_{\mathrm{FDE}(6)}(\boldsymbol{r}) + \rho^{(2)}_{\mathrm{FDE}(6)}(\boldsymbol{r})))\boldsymbol{r}d\boldsymbol{r}; \tag{15}$$

the integrated absolute difference density,

$$\Delta^{\mathrm{abs}} = \frac{1}{N}\int |(\rho^{\mathrm{KS}}(\boldsymbol{r}) - (\rho^{(1)}_{\mathrm{FDE}(6)}(\boldsymbol{r}) + \rho^{(2)}_{\mathrm{FDE}(6)}(\boldsymbol{r})))|d\boldsymbol{r}; \tag{16}$$

and the root-mean-square error in the density,

$$\Delta^{\mathrm{rms}} = \frac{1}{N}\sqrt{\int (\rho^{\mathrm{KS}}(\boldsymbol{r}) - (\rho^{(1)}_{\mathrm{FDE}(6)}(\boldsymbol{r}) + \rho^{(2)}_{\mathrm{FDE}(6)}(\boldsymbol{r})))^2 d\boldsymbol{r}}. \tag{17}$$

Here, $\rho^{\mathrm{KS}}(\boldsymbol{r})$ is the density of the supermolecule obtained with the conventional KS method, $\rho^{(1)}_{\mathrm{FDE}(6)}(\boldsymbol{r})$ and $\rho^{(2)}_{\mathrm{FDE}(6)}(\boldsymbol{r})$ are the densities obtained with the FDE scheme, and N is the total number of electrons of the systems under investigation. These data are presented in Table II for the molecules Ar–AuF, Kr–AuF, and Xe–AuF, respectively. The "sum of fragments" designates the superposition of the densities obtained by KS calculations on the isolated fragments (Ng and AuF). This is the starting density on which the FDE scheme is expected to improve upon. The dipole moments of AuF, Ar–AuF, Kr–AuF, and Xe–AuF are 3.61, 5.47, 5.76, and 6.28 D, respectively. It can be seen that the relative accuracy drops when one moves from Ar to Xe for all functionals, except for PBE2 and PBE3 when going from Ar to Kr. This overall loss in accuracy is expected given the increase in covalent character of the bond between the Ng and AuF upon moving from Ar to Xe. This drop in accuracy is hardly visible for Δ^{rms} because, compared with Δ^{abs}, this measure puts

TABLE II. The dipole moment difference $\Delta\mu$ in debye, the integrated absolute difference density Δ^{abs}, and root-mean-square error in the density Δ^{rms} for Ar–AuF, Kr–AuF, and Xe–AuF. All the data refer to the comparison to KS-DFT. All FDE calculations are done in the monomolecular expansion FDE(m).

	Ar–AuF			Kr–AuF			XeAuF		
	$\Delta\mu$	$\Delta^{\mathrm{abs}}\times 10^3$	$\Delta^{\mathrm{rms}}\times 10^3$	$\Delta\mu$	$\Delta^{\mathrm{abs}}\times 10^3$	$\Delta^{\mathrm{rms}}\times 10^3$	$\Delta\mu$	$\Delta^{\mathrm{abs}}\times 10^3$	$\Delta^{\mathrm{rms}}\times 10^3$
Sum of fragments	1.80	4.04	0.41	2.15	4.29	0.39	2.67	4.61	0.41
TF	1.04	3.87	0.44	1.24	4.07	0.43	1.86	4.67	0.45
TF9W	1.07	3.48	0.40	1.11	3.59	0.39	1.59	4.23	0.42
PW91K	1.10	3.52	0.39	1.19	3.63	0.39	1.75	4.30	0.41
TW02	1.12	3.49	0.39	1.22	3.59	0.38	1.79	4.22	0.41
PBE2	1.74	4.94	0.47	0.97	4.25	0.41	1.25	4.83	0.44
PBE3	2.36	9.48	1.00	2.45	9.43	0.97	7.16	14.98	1.32
PBE4	7.46	26.12	2.83	8.13	24.49	2.09	12.33	25.91	2.25

more weight on the nuclear regions of gold where the density and error do not change so much through the series.

As expected, TF, TF9W, PW91K, and TW02 functionals all improve the sum of fragments starting density, although the magnitude of this improvement is small. Considering only the dipole moment difference, the TF9W model appears to yield the best results. Regarding the other two measures of accuracy, the TW02 functional performs best. In general the differences in results between these functionals are rather small, especially compared with the absolute size of the errors that amount to more than 1 D in the dipole moment. The popular PW91K functional gives in this case less accurate results than TF9W and TW02.

It is noteworthy that for PBE*n* functionals, results with six FT cycles shown in Table II are worse than one would expect from the results without FT cycles shown in Table I. This is due to significant changes in the AuF density during FT cycles. Among others, the dipole moment of the AuF unit changes significantly (1.02, 0.91, and 1.00 D for ArAuF, KrAuF, and XeAuF, respectively) when employing these functionals contrary to what is to be expected on basis of the weak intermolecular interaction and the strong intramolecular interaction. After FT cycles the PBE2 and PBE3 functionals now yield worse results than the other conjointness functionals, with PBE2 only slightly improving over the sum of fragments. The larger departure from the TF reference used in the PBE*n* functionals does thus lead to artifacts when the frozen density is allowed to relax. This is also the cause of the convergence problems observed in the FDE(s) calculations in which the full AuF basis is available in the noble gas subsystem calculation. A similar behavior has been observed in our earlier work for other functionals,[21,36] among which also the PW91K functional. This can be remedied to some extent by either cutting off the core regions of the potential using a switching function[36] or by allowing for a KE functional that is no longer decomposable into two separate contributions from the total and active densities.[37] As both approaches are only valid in the limit of nonoverlapping densities we will not consider them here in detail. Exploratory calculations with the switching function used in reference[36] do not show improvement of results obtained with PBE2 after FT, increasing the underestimation of the dipole moment from 1.74 to 1.87 D. This was expected since the switching function is constructed to test for a small overlap situation and will not fully activate the correction in the current case.

The PBE3 and PBE4 functionals are not suitable for use in a full optimization scheme that includes FT relaxation cycles. For these functionals all measures of accuracy deteriorate as compared with the sum of fragments starting density. Also for PBE2, while still yielding an acceptable final result, the use of FT cycles will lead to deterioration rather than an improvement of the promising results (cf. Table I) that are obtained without this relaxation.

V. CONCLUSIONS

The effective-embedding potentials produced by the currently available KE density functionals for use in the FDE method appear to be too repulsive to properly describe the coordination bonding found in the noble gas atom bound to the gold fluoride molecule. The use of increasing orders of the reduced density gradient s in the expression of GGA KE functionals does not necessarily yield improved functionals, as can be seen from the bad performance of the PBE4 functional. This could, however, be an effect of the chosen parametrization that was developed for a quite different purpose and bonding situation. The performance of a given GGA functional varies significantly depending on the location on the bond axis. For example, the density obtained with the PBE3 functional follows the KS trend closely near the Ar and F atoms, whereas in the bonding region and near the Au atom it fails.

The general conclusion is that for systems like NgAuF (Ng=Ar, Kr, Xe), none of the enhancement functions used in the approximate KE functionals is yet able to describe the weak covalent bond adequately. The PBE2 functional comes closest to the KS result, but can only be used with a frozen AuF unit as updating the AuF density worsens the result. But also functionals with a proven accuracy in other bonding situations, like PW91K, fail for this more challenging bonding situation. It is important to note that GGA functionals, such as PW91k, are able to accurately describe much stronger bonds, such as the hydrogen bond in $F-H-F^-$.[29] Therefore, the bond strength alone is not a sufficient criterion to judge whether GGA functionals can be expected to yield an adequate description, one also needs some *a priori* knowledge of the bonding characteristics.

The failure of GGA KE functionals even for weak covalent bonds raises the question as to whether the conjointness approach as applied in previous work is suitable to derive functionals that can describe the stronger interactions, which are of interest in many applications of subsystem methods.[68] It could be interesting to approximate the KE component of the embedding potential directly in a nondecomposable fashion[36,37] also in regions in which the frozen and active densities show a significant overlap. An alternative is to introduce approximations that not only locally depend on the electron densities of the subsystems, but that also depend on the KS orbitals of the subsystems. This would make the method similar to a pseudopotential approach in which the orbital information is also used to model the effect of the frozen density.

ACKNOWLEDGMENTS

This work has been supported by the Netherlands Organization for Scientific Research (NWO) in form of a Vici grant for L.V. C.R.J. acknowledges funding by a Rubicon scholarship of NWO.

[1] F. Maseras and K. Morokuma, J. Comput. Chem. **16**, 1170 (1995).
[2] K. Kitaura, Chem. Phys. Lett. **313**, 701 (1999).
[3] D. W. Zhang and J. Z. H. Zhang, J. Chem. Phys. **119**, 3599 (2003).
[4] R. P. A. Bettens and A. M. Lee, J. Phys. Chem. A **110**, 8777 (2006).
[5] H. M. Senn and W. Thiel, Angew. Chem., Int. Ed. **48**, 1198 (2009).
[6] A. Warshel and M. Levitt, J. Mol. Biol. **103**, 227 (1976).
[7] N. Vaidehi, T. A. Wesolowski, and A. Warshel, J. Chem. Phys. **97**, 4264 (1992).
[8] T. A. Wesolowski and A. Warshel, J. Phys. Chem. **97**, 8050 (1993).

[9] J. Neugebauer, M. J. Louwerse, E. J. Baerends, and T. A. Wesolowski, J. Chem. Phys. **122**, 094115 (2005).
[10] C. R. Jacob, J. Neugebauer, L. Jensen, and L. Visscher, Phys. Chem. Chem. Phys. **8**, 2349 (2006).
[11] R. E. Bulo, C. R. Jacob, and L. Visscher, J. Phys. Chem. A **112**, 2640 (2008).
[12] M. E. Casida and T. A. Wesolowski, Int. J. Quantum Chem. **96**, 577 (2004).
[13] J. Neugebauer, J. Chem. Phys. **126**, 134116 (2007).
[14] M. Zbiri, M. Atanasov, C. Daul, J. M. Garcia-Lastra, and T. A. Wesolowski, Chem. Phys. Lett. **397**, 441 (2004).
[15] J. Neugebauer, C. R. Jacob, T. A. Wesolowski, and E. J. Baerends, J. Phys. Chem. A **109**, 7805 (2005).
[16] J. Neugebauer, J. Phys. Chem. B **112**, 2207 (2008).
[17] A. S. P. Gomes, C. R. Jacob, and L. Visscher, Phys. Chem. Chem. Phys. **10**, 5353 (2008).
[18] M. Dulak and T. A. Wesolowski, Int. J. Quantum Chem. **101**, 543 (2005).
[19] T. A. Wesolowski, Y. Ellinger, and J. Weber, J. Chem. Phys. **108**, 6078 (1998).
[20] T. A. Wesolowski, J. Chem. Phys. **106**, 8516 (1997).
[21] A. W. Götz, S. M. Beyhan, and L. Visscher, J. Chem. Theory Comput. **5**, 3161 (2009).
[22] M. Dułak, J. W. Kaminski, and T. A. Wesolowski, J. Chem. Theory Comput. **3**, 735 (2007).
[23] M. Štrajbl, G. Hong, and A. Warshel, J. Phys. Chem. B **106**, 13333 (2002).
[24] M. Iannuzzi, B. Kirchner, and J. Hutter, Chem. Phys. Lett. **421**, 16 (2006).
[25] S. C. L. Kamerlin, M. Haranczyk, and A. Warshel, J. Phys. Chem. A **113**, 1253 (2009).
[26] P. Cortona, Phys. Rev. B **44**, 8454 (1991).
[27] C. R. Jacob and L. Visscher, J. Chem. Phys. **128**, 155102 (2008).
[28] T. A. Wesolowski, in *Computational Chemistry: Reviews of Current Trends*, edited by J. Leszczynski (World Scientific, Singapore, 2006), Vol. 10.
[29] K. Kiewisch, G. Eickerling, M. Reiher, and J. Neugebauer, J. Chem. Phys. **128**, 044114 (2008).
[30] T. A. Wesolowski and J. Weber, Chem. Phys. Lett. **248**, 71 (1996).
[31] T. A. Wesolowski, H. Chermette, and J. Weber, J. Chem. Phys. **105**, 9182 (1996).
[32] T. A. Wesolowski and J. Weber, Int. J. Quantum Chem. **61**, 303 (1997).
[33] C. R. Jacob, T. A. Wesolowski, and L. Visscher, J. Chem. Phys. **123**, 174104 (2005).
[34] F. Tran, J. Weber, and T. A. Wesolowski, Helv. Chim. Acta **84**, 1489 (2001).
[35] S. Fux, K. Kiewisch, C. R. Jacob, J. Neugebauer, and M. Reiher, Chem. Phys. Lett. **461**, 353 (2008).
[36] C. R. Jacob, S. M. Beyhan, and L. Visscher, J. Chem. Phys. **126**, 234116 (2007).
[37] J. M. Garcia Lastra, J. W. Kaminski, and T. A. Wesolowski, J. Chem. Phys. **129**, 074107 (2008).
[38] H. Lee, C. Lee, and R. G. Parr, Phys. Rev. A **44**, 768 (1991).
[39] V. V. Karasiev, S. B. Trickey, and F. E. Harris, J. Comput.-Aided Mater. Des. **13**, 111 (2006).
[40] S. A. Cooke and M. C. L. Gerry, J. Am. Chem. Soc. **126**, 17000 (2004).
[41] L. Belpassi, I. Infante, F. Tarantelli, and L. Visscher, J. Am. Chem. Soc. **130**, 1048 (2008).
[42] L. H. Thomas, Math. Proc. Cambridge Philos. Soc. **23**, 542 (1927).
[43] E. Fermi, Atti Accad. Naz. Lincei, Cl. Sci. Fis., Mat. Nat., Rend. **6**, 602 (1927).
[44] E. H. Lieb, Rev. Mod. Phys. **53**, 603 (1981).
[45] E. Teller, Rev. Mod. Phys. **34**, 627 (1962).
[46] N. L. Balàzs, Phys. Rev. **156**, 42 (1967).
[47] E. H. Lieb and B. Simon, Phys. Rev. Lett. **31**, 681 (1973).
[48] E. H. Lieb and B. Simon, Adv. Math. **23**, 22 (1977).
[49] C. F. von Weizsäcker, Z. Phys. **96**, 431 (1935).
[50] A. Lembarki and H. Chermette, Phys. Rev. A **50**, 5328 (1994).
[51] D. J. Lacks and R. G. Gordon, J. Chem. Phys. **100**, 4446 (1994).
[52] P. Fuentealba and O. Reyes, Chem. Phys. Lett. **232**, 31 (1995).
[53] P. Fuentealba, J. Mol. Struct. **390**, 1 (1997).
[54] F. Tran and T. A. Wesolowski, Int. J. Quantum Chem. **89**, 441 (2002).
[55] J. P. Perdew, Phys. Lett. A **165**, 79 (1992).
[56] J. P. Perdew, in *Electronic Structure of Solids*, edited by P. Ziesche and H. Eschrig (Akademie, Berlin, 1991), pp. 11–20.
[57] J. P. Perdew, K. Burke, and M. Ernzerhof, Phys. Rev. Lett. **77**, 3865 (1996).
[58] C. Adamo and V. Barone, J. Chem. Phys. **116**, 5933 (2002).
[59] C. R. Jacob, J. Neugebauer, and L. Visscher, J. Comput. Chem. **29**, 1011 (2008).
[60] G. te Velde, F. M. Bickelhaupt, E. J. Baerends, C. Fonseca Guerra, S. J. A. van Gisbergen, J. G. Snijders, and T. Ziegler, J. Comput. Chem. **22**, 931 (2001).
[61] ADF2008.01, SCM, Theoretical Chemistry, Vrije Universiteit, Amsterdam, The Netherlands, http://www.scm.com, accessed on May 2008.
[62] E. van Lenthe, E. J. Baerends, and J. G. Snijders, J. Chem. Phys. **99**, 4597 (1993).
[63] E. van Lenthe, E. J. Baerends, and J. G. Snijders, J. Chem. Phys. **101**, 9783 (1994).
[64] C. J. Evans, D. S. Rubinoff, and M. C. L. Gerry, Phys. Chem. Chem. Phys. **2**, 3943 (2000).
[65] J. M. Thomas, N. R. Walker, S. A. Cooke, and M. C. L. Gerry, J. Am. Chem. Soc. **126**, 1235 (2004).
[66] B. P. Tripathi, R. K. Laloraya, and S. L. Srivasta, Phys. Rev. A **6**, 850 (1972).
[67] Y. A. Bernard, M. Dulak, J. W. Kaminski, and T. A. Wesolowski, J. Phys. A: Math. Theor. **41**, 055302 (2008).
[68] C. R. Jacob and L. Visscher, in *Recent Advances in Orbital-Free Density Functional Theory*, edited by Y. A. Wang and T. A. Wesolowski (World Scientific, Singapore, 2010).